Optical properties of a multiple quantum well in a HgTe/CdTe system

1996 J. Phys.: Condens. Matter 8 7619

(http://iopscience.iop.org/0953-8984/8/41/010)

J. Phys.: Condens. Matter **8** (1996) 7619–7636. Printed in the UK

Optical properties of a multiple quantum well in a HgTe/CdTe system

Suck-Whan Kim† and Ki-Soo Sohn‡

† Department of Physics, Andong National University, Andong 760-749, South Korea
‡ Department of Physics, Kyungpook National University, Taegu 702-701, South Korea

Received 12 January 1996, in final form 2 July 1996

Abstract. A finite HgTe/CdTe superlattice with different dielectric media on either side of the surfaces is investigated by taking into account the wavefunction overlap between the interface states and plasmons. The unit cell of the finite HgTe/CdTe superlattice consists of two electron-like states and a heavy-hole-like state in HgTe and two light-hole-like states in CdTe. Using the random-phase approximation added with some assumptions, we have studied the density–density correlation function by considering the interface state with the wavefunctions overlapping with the electron-like states, the light-hole-like states and the heavy-hole-like states. We have calculated the collective excitation spectra of the intrasubband and the intersubband for both the bulk plasmons and the surface plasmons as a function of the number of unit cells. The Raman intensities due to bulk and surface plasmons are expressed by the relative value of the mode energy of the plasmons.

1. Introduction

In recent years there has been increasing interest in the investigation of artificial low-dimensional semiconductor structures. The quantum confinement of electrons and holes in these structures strongly modifies the electronic properties (Esaki and Tsu 1970), which play an important role in the performance of optoelectronic devices. Most of the theoretical and experimental studies have been performed on either type-I superlattices (Chang and Esaki 1980, Dingle *et al* 1980, Olego *et al* 1982, Giuliani and Quinn 1984, Tselis and Quinn 1984, Hawrylak *et al* 1985a, b, Jain and Allen 1985a, b, Sooryakumar *et al* 1985, Das Sarma and Quinn 1986 and Pinczuk *et al* 1986) or type-II superlattices (Hawrylak *et al* 1986, Tzoar and Zhang 1986). The structures of the subbands have been studied by the far-infrared absorption spectroscopy and the resonant-light-scattering technique. From a theoretical viewpoint, the important things required to understand the superlattice, which is an ideal structure for studying electrical and optical properties, are the elementary excitations of these systems (Grecu 1973, Fetter 1974). Recently, much attention has been given to the HgTe/CdTe system superlattice (Chang *et al* 1985, Guldner *et al* 1985, Lin-Lin and Sham 1985, Berrior *et al* 1986, Faurie 1986, Jaros *et al* 1987, Huang and Zhou 1988, Huang *et al* 1989) which consists of a semimetal and semiconductor. The band structures of a HgTe/CdTe superlattice calculated by the plane-wave method (Mukherji and Nag 1957), the linear-combination-of-atomic-orbitals method (Chang *et al* 1985, Jaros *et al* 1987), and the envelope-function-approximation methods show that they can be either semiconducting or zero-band-gap semiconductors and that the electron-like and heavy-hole-like states in HgTe layers, and the light-hole-like states in CdTe layers, are very well confined (Berrior *et al*

0953-8984/96/417619+18$19.50

1986, Faurie 1986, Jaros *et al* 1987), respectively. Moreover, these methods show that the interface states are localized near the interfaces (Chang *et al* 1985, Lin-Lin and Sham 1985). The fact that the width of the band gap strongly depends on the hybridization of interface states with the heavy-hole-like subbands implies that the interface states are important in studying the properties of the HgTe/CdTe superlattice such as optical absorption, transport and collective excitation (Berrior *et al* 19865, Faurie 1986, Jaros *et al* 1987). The optical properties for the carriers in the HgTe/CdTe superlattice are modelled on the experimental and theoretical results of charge densities of carriers in the HgTe and CdTe cells (Berrior *et al* 1986, Faurie 1986, Jaros *et al* 1987).

In this paper the collective-excitation spectra of plasmons for surface bulk states are investigated as a function of the number of unit cells in a simplified HgTe/CdTe superlattice model. The main emphasis is on the effects of overlap between interface states and other plasmons and the Raman intensity versus the relative value of energy states such as electron-like states, light-hole-like states and heavy-hole-like state. It is assumed that HgTe and CdTe layers in a unit cell have the same thickness. Electron-like states in HgTe layers are assumed to be confined in a quantum well of thickness L_E which is measured from the edge of the HgTe layer (Huang and Zhou 1988, Huang *et al* 1989). Light-hole-like states in CdTe layers are assumed to be confined in a quantum well of thickness L_L which is measured from the edge of the CdTe layer, and it is assumed that heavy-hole-like states in HgTe layers are confined in a quantum well of thickness L_H in the middle of the HgTe layer.

The motion of carriers in the X–Y plane is assumed to be completely free and the tunnelling of carriers between adjacent interface states is neglected. We also assume that only the first and second subbands of plasmon states in both the HgTe layer and the CdTe layer are occupied in equilibrium. The centres of the electron-like states confined in the quantum well of thickness L_E in HgTe layers are located at $z = ld + L_E/2$ and $z = (l + \frac{1}{2})d - L_E/2$ and those of the light-hole-like states confined in the quantum well of thickness L_L in CdTe layers are located at $z = (l + \frac{1}{2})d + L_L/2$ and $z = (l + 1)d - L_L/2$, where l goes from 0 to $N - 1$. The centres of the heavy-hole-like states confined in the quantum well of thickness L_H in HgTe layers (Huang *et al* 1989) are located at $z = (l+\frac{1}{4})d$. The electron-like states, the light-hole-like states and the heavy-hole-like states are confined in a semi-infinite array of quantum wells embedded in a space of dielectric constant ε where $z > -\delta$.

In section 2, the density–density correlation function is derived under the random-phase approximation for semi-infinite space (Kim and Sohn 1994) described above. Calculations are carried out analytically as far as possible. We here include the intersubband scattering of incoming light with the electron-light state and the heavy-hole-like states in HgTe layers and the light-hole-like state in CdTe layers. In section 3, dispersion spectra (Kim and Sohn 1994) of the surface and bulk plasmon for infinite layers are calculated. Dispersion spectra of the bulk plasmons are also calculated as a function of the number of unit cells for various carriers. In section 4, the Raman intensity is calculated analytically in terms of the density–density correlation function, and these Raman spectra are analysed as a function of ω/ω_E. Section 5 concludes our work.

2. Density–density correlation function

The model system of N unit cells, each of which contains two layers, HgTe and CdTe layers, has $2N$ and N quantum wells for the electron-like and the heavy-hole-like states, respectively, in the HgTe layers, and $2N$ quantum wells for the light-hole-like states in the

CdTe layers. The particle states in the unit cell are assumed to be of the form (Kim and Sohn 1994)

$$|qln\rangle = \exp(\mathrm{i}\boldsymbol{q}\cdot\boldsymbol{r})\,\zeta_{ln}(z) \tag{1}$$

where

$$\zeta_{ln}(z) = [\xi_n^E(z-ld) + \xi_n^E(z-(l+\tfrac{1}{2})d) + \xi_n^H(z-(l+\tfrac{1}{4})d) + \xi_n^L(z-(l+\tfrac{1}{2})d) + \xi_n^L(z-(l+1)d) + \xi_c^I(z-(l+\tfrac{1}{2})d)]\exp(\mathrm{i}k_z la) \tag{2}$$

where $\xi_n^E(z-ld)$ and $\xi_n^E(z-(l+\frac{1}{2})d)$ are the electron-like wavefunctions at both edges in the HgTe layer, $\xi_n^H(z-(l+\frac{1}{4})d)$ is the heavy-hole-like wavefunction in the HgTe layer, $\xi_n^L(z-(l+\frac{1}{2})d)$ and $\xi_n^L(z-(l+1)d)$ are the light-hole-like wavefunctions at both edges in the CdTe layer, $\xi_c^I(z-(l+\frac{1}{2})d)$ is the interface state wavefunction, q is the momentum in the layer perpendicular to the z axis, and $n = 0, 1, \ldots, m-1$ is the subband index. Here, the subscript c of the function ξ_c^I can be selected to be either A or S. A and S represent the antisymmetric wavefunction and the symmetric wavefunction, respectively, at interface states. These wavefunctions are considered to be real.

In the random-phase approximation (Grecu 1973, Fetter 1974), $\Pi_{nmn'm'}(l, l_1, l', l_1')$ satisfies the integral equations

$$\Pi_{n,m,n',m'}(l,l') = \sum_{l_1,l_1'} \Pi_{n,m,n',m'}(l,l_1,l',l_1') \tag{3}$$

and

$$\Pi_{n,m,n',m'}(l,l') = \Pi^0_{nm}\delta_{nn'}\delta_{mm'}\delta_{ll'} + \sum_{l',r,s} \Pi^0_{nm} V_{nm,rs}(l,l'')\Pi_{rs,n'm'}(l'',l') \tag{4}$$

where Π^0_{nm}, the polarizability of the non-interacting system, which is due to the polarizability between one zeroth subband which overlaps with the nth subband, and another zeroth subband which overlaps with the mth subband, is layer independent (Hawrylak *et al* 1986). $V_{nm,rs}(l,l')$ is the Coulomb interaction between the layers in the unit cells, including the effect of image charges and subband structure (Grecu 1973, Hawrylak *et al* 1985a, b, Eliasson *et al* 1987, Kim and Sohn 1994):

$$V_{nm,n'm'}(l,l') = \sum_{l_1,l_1'} V_q \int_{-\delta}^{\infty} \mathrm{d}z \int_{-\delta}^{\infty} \mathrm{d}z'\,\zeta^*_{ln}(z)\zeta_{l_1m}(z)\{\exp(-q|z-z'|) + \alpha_0\exp[-q(z+z')]\}\zeta_{l'n'}(z')\zeta^*_{l',m'}(z') \tag{5}$$

where $\alpha_0 = [(\varepsilon-\varepsilon_0)/(\varepsilon+\varepsilon_0)]\exp(-2\delta q)$, $\varepsilon = \varepsilon_\infty(\omega^2-\omega_l^2+\mathrm{i}\gamma_0\omega)/(\omega^2-\omega_T^2+\mathrm{i}\gamma_0\omega)$ and $V_q = 2\pi e^2/\varepsilon q$. ω_l and ω_T are the longitudinal- and transverse-optical-phonon frequencies, respectively, and γ_0 is the phenomenological broadening.

Equation (5) can be rewritten as

$$V_{nm,nm}(l,l') = \sum_{l_1,l_1'} \sum_{i,j,t,w} V^{ijtw}_{nm,nm}(l,l_1,l',l_1') \tag{6}$$

where $V^{ijtw}_{nm,n'm'}(l,l_1,l',l_1')$ expressed by the density–density correlation function of the particle states in units cells is given in appendix 2.

By defining a dielectric matrix $\varepsilon(l,l';nm)$, and using self-consistent linear-density-response theory, equation (4) can be transformed into

$$\varepsilon(l,l';nm) = \delta_{nn'}\delta_{mm'}\delta_{ll'} - \Pi^0_{nm}V_{nm,nm}(l,l') \tag{7}$$

and then the elements of the polarizability matrix are $\Pi_{nm} = \Pi^0_{nm}\varepsilon(l,l';nm)^{-1}$. We decompose $V^{ijtw}_{nm,n'm'}(k_z,k'_z)$ and $\Pi^{ijtw}_{nm,n'm'}(k_z,k'_z)$ obtained by the Fourier transform of $V_{nm,nm}(l,l')$ and $\Pi^{ijtw}_{nm,n'm'}(l,l')$ into the bulk part and the surface part (Hawrylak *et al* 1985a, b, 1986, Eliasson *et al* 1987) and rewrite $\Pi^{ijtw}_{nm,n'm'}(k_z,k'_z)$ as a matrix $\mathbf{\Pi}(k_z,k'_z)$. Then the equation gives two coupled equations of $\mathbf{\Pi}_B$ (Kim and Sohn 1994) and $\mathbf{\Pi}_S$.

$\mathbf{\Pi}_S(k_z,k'_z)$ is finally expressed by

$$\begin{aligned}\mathbf{\Pi}_S(k_z,k'_z) = {} & \frac{[1-\exp(-qdN)]\mathbf{\Pi}_B(k_z)}{4NP(k_z)P(k'_z)}[R^*_{k_z,n}R_{k_z,m} - (\delta_{i,E}\delta_{j,E} + \delta_{i,L}\delta_{j,L} + \delta_{i,H}\delta_{j,H}) \\ & \times(R_{k_z,n}R^*_{k_z,m} - 1)][R^*_{k'_z,n'}R_{k'_z,m'} - (\delta_{t,E}\delta_{w,E} + \delta_{t,L}\delta_{w,L} + \delta_{t,H}\delta_{w,H}) \\ & \times(R_{k'_z,n'}R^*_{k'_z,m'} - 1)]\{A_{11} + A_{12}\exp(-\mathrm{i}k'_z d) + A_{21}\exp(\mathrm{i}k_z d) \\ & + A_{22}\exp[\mathrm{i}(k_z - k'_z)d]\}\mathbf{\Pi}_B(k'_z) \qquad (8)\end{aligned}$$

where $P(k_z) = \cosh(qd) - \cos(k_z d)$ and the renormalization coefficient $R_{k_z,n}$ is given in appendix 2. Combination of the equations for $\mathbf{\Pi}_B$ and $\mathbf{\Pi}_S$ results in a matrix equation for $M(q,\omega)$ with coefficients A_{11}, A_{12}, A_{21} and A_{22} (Grecu 1973, Hawrylak *et al* 1985a, b, Eliasson *et al* 1987).

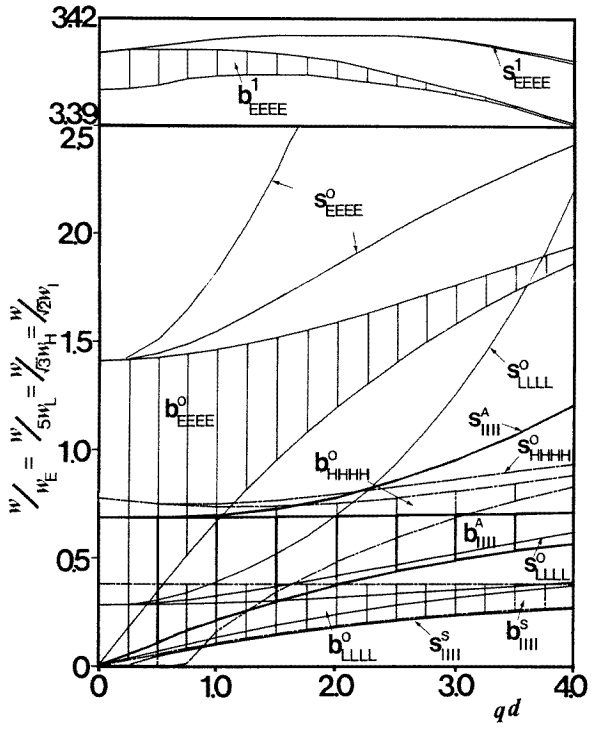

Figure 1. Dispersion relation $\omega/\omega_E = \omega/5\omega_L = \omega/\sqrt{3}\omega_H = \omega/\sqrt{2}\omega_I$ versus qd for the intrasubband and intersubband plasmon modes contributed by $EEEE$, $LLLL$, $HHHH$ and $IIII$ states using the symmetric and antisymmetric wavefunctions at the interface states. The parameters are as follows; $n = 12.8\times10^{12}$ cm^{-2}, $d = 80$ Å, $L_E = d/8$, $L_L = d/8$, $L_H = d/10$, $2\delta = d$, $m_i = 0.7m_e$, $\varepsilon_\infty = 16$, $\varepsilon_0 = 1.0$, $k = 0.747/d$ (Eliasson *et al* 1987, Huang and Zhou 1988, Huang *et al* 1989, Kim and Sohn 1994) and $\gamma_i/\omega_i = 0.2$ with $i = E$, L, H and I.

3. Bulk plasmons

We consider the dispersion spectra of the collective modes in a few cases. Poles of the density–density correlation function $\mathbf{\Pi}(k_z, k_z')$ define the collective excitations of the superlattice (Grecu 1973, Fetter 1974). For a finite number of layers a full solution must be used. The bulk plasmons are given by the poles of the bulk part while the surface plasmons are given by the poles of the surface part. During the calculation, it is assumed that the electron-like function and the heavy-hole-like function in the HgTe layer and the light-hole-like wavefunction in the CdTe layer (Huang and Zhou 1988) are

$$\begin{aligned}\xi_n^i\left(z - ld - \frac{\delta_{i,E}d}{2}(1-\theta) - \frac{\delta_{i,L}d}{2}(1+\theta) - \frac{\delta_{i,H}d}{4}\right) &= \sqrt{\frac{2}{L_i}}\sin\left[\left(\frac{n+1}{L_i}\pi\right)\right. \\ &\times(z-ld) - \delta_{i,E}\left(\frac{d}{2} - L_i\right)(1-\theta) - \delta_{i,L}\left(\frac{d}{2}(1+\theta) - L_i\theta\right) \\ &\left.-\delta_{i,H}\left(\frac{d}{4} - \frac{L_i}{2}\right)\right], ld + \delta_{i,E}\left(\frac{d}{2}(1-\theta) - L_i(1-\theta)\right) \\ &+\delta_{i,L}\left(\frac{d}{2}(1+\theta) - L_i\theta\right) + \delta_{i,H}\left(\frac{d}{4} - \frac{L_i}{2}\right) < z < ld \\ &+\delta_{i,E}\left(\frac{d}{2}(1-\theta) + L_i\theta\right) + \delta_{i,L}\left(\frac{d}{2}(1+\theta) - L_i(\theta-1)\right) + \delta_{i,H}\left(\frac{d}{4} + \frac{L_i}{2}\right) \\ &\text{for } n = 0, 1 \text{ and } i = E, H \text{ or } L \end{aligned} \tag{9}$$

where θ is the step function. The symmetric and antisymmetric wavefunctions at interface state are chosen as the following:

$$\xi_S^I(z - (l+\tfrac{1}{2})d)$$
$$= \begin{cases} R_S\{\exp[k(z-ld)] + \exp[-k(z-ld)]\} & ld < z < (1+\frac{1}{4})d \\ R_S(\exp\{-k[z-(1+\frac{1}{2})d]\} + \exp\{k[z-(l+\frac{1}{2})d]\}) & (l+\frac{1}{4})d < z < (l+\frac{3}{4})d \\ R_S(\exp\{k[z-(l+1)d]\} + \exp\{-k[z-(l+1)d]\}) & (l+\frac{3}{4})d < z < (l+1)d \end{cases} \tag{10}$$

and

$$\xi_A^I(z - (l+\tfrac{1}{2})d)$$
$$= \begin{cases} R_A\{\exp[k(z-ld)] - \exp[-k(z-ld)]\} & ld < z < (l+\frac{1}{4})d \\ R_A(\exp\{-k[z-(l+\frac{1}{2})d]\} - \exp\{k[z-(l+\frac{1}{2})d]\}) & (l+\frac{1}{4})d < z < (l+\frac{3}{4})d \\ R_A(\exp\{k[z-(l+1)d]\} - \exp\{-k[z-(l+1)d]\}) & (l+\frac{3}{4})d < z < (l+1)d \end{cases} \tag{11}$$

where $R_S = \{[4\sinh(kd/2)]/k + 2d\}^{-1/2}$ and $R_A = \{[4\sinh(kd/2)]/k - 2d\}^{-1/2}$. Here we set $k_{HgTe} = k_{CdTe} = k$ in the calculation for simplicity. It is defined that $\varepsilon(k_z) = \mathbf{\Pi}^0(k_z)/\mathbf{\Pi}^B(k_z)$. The pole of $\mathbf{\Pi}^B(k_z)$ which is the roots of $\varepsilon(k_z) = 0$ leads to the dispersion relation of the bulk plasmon. The background dielectric values (Hawrylak *et al* 1985a, b, Huang and Zhou 1988) are given as $\varepsilon_\infty = 16$ and $\varepsilon_0 = 1$. The distance from the first layer to the interface of the other half-space is $\delta = d/2$. The polarizability in the long-wavelength limit is given by (Kim and Sohn 1994)

$$\Pi_{00}^{0iiii} = \frac{n_i q^2}{m_i(\omega^2 + \mathrm{i}\gamma_i\omega)} \qquad (i = E, L, H \text{ or } I) \tag{12}$$

$$\Pi_{10}^{0iii} = \frac{2n_i E_{i10}}{\omega^2 - E_{i10}^2 + \mathrm{i}\gamma_i\omega} \qquad (i = E, L \text{ or } H) \tag{13}$$

and Π_{00}^{0EEII}, Π_{00}^{0LLII}, Π_{00}^{0HHII}, Π_{00}^{0EEEI}, Π_{00}^{0LLLI} and Π_{00}^{0HHHI} are defined as the following:

$$\Pi_{00}^{0EEII} = (\Pi_{00}^{0EEEE})^{1/2}(\Pi_{00}^{0IIII})^{1/2} f \qquad (f = \alpha_{01} \text{ and } \alpha_{02}) \tag{14}$$

$$\Pi_{00}^{0LLII} = (\Pi_{00}^{0LLLL})^{1/2}(\Pi_{00}^{0IIII})^{1/2} f \qquad (f = \beta_{01} \text{ and } \beta_{02}) \tag{15}$$

$$\Pi_{00}^{0HHII} = (\Pi_{00}^{0HHHH})^{1/2}(\Pi_{00}^{0IIII})^{1/2}\gamma_{nc} \tag{16}$$

$$\Pi_{00}^{0EEEI} = (\Pi_{00}^{0EEEE})^{3/4}(\Pi_{00}^{0IIII})^{1/4} f \qquad (f = \alpha_{01} \text{ and } \alpha_{02}) \tag{17}$$

$$\Pi_{00}^{0LLLI} = (\Pi_{00}^{0LLLL})^{3/4}(\Pi_{00}^{0IIII})^{1/4} f \qquad (f = \beta_{01} \text{ and } \beta_{02}) \tag{18}$$

and

$$\Pi_{00}^{0HHHI} = (\Pi_{00}^{0HHHH})^{3/4}(\Pi_{00}^{0IIII})^{1/4}\gamma_{nc}. \tag{19}$$

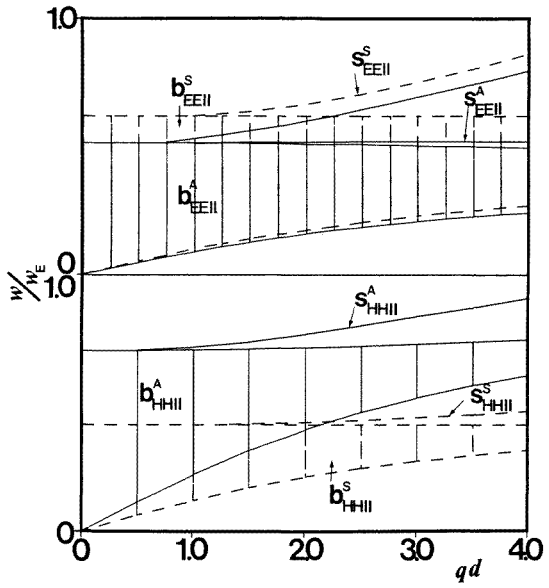

Figure 2. Dispersion relation $\omega/\omega_E = \omega/5\omega_L = \omega/\sqrt{3}\omega_H = \omega/\sqrt{2}\omega_I$ versus qd for the intrasubband bulk and surface plasmons modes contributed by $EEII$ (upper section) and (b) $HHII$ (lower section) states using the symmetric and antisymmetric wavefunctions at the interface states. The parameters used are the same as in figure 1.

Π_{00}^{0IIEI}, Π_{00}^{0IILI} and Π_{00}^{0IIHI} can be expressed in similar forms. γ_i is the phenomenological broadening of electron-like states, light-hole-like states, heavy-hole-like states or interface states. γ_{nc} is the coefficient of the overlap between the heavy-hole-like states and interface states. The plasma frequency ratios of the electron-like states to the light-hole-like states, the electron-like states to the heavy-hole-like states, and the electron-like states to the interface state are $\omega_E^2/\omega_L^2 = 25$, $\omega_E^2/\omega_H^2 = 3$ and $\omega_E^2/\omega_I^2 = 2$, respectively, at $\omega_i = (2\pi n_i e^2/m_i\varepsilon a)^{1/2}$. Here a single-particle energy separation is given by $E_{i10}/\omega_i = 2.5$ for $i = E, L$ or H. For convenience we shall denote the wavefunctions by superscripts as $\xi_0^E(z-ld)\xi_0^E(z-ld)\xi_0^E(z'-l'd)\xi_0^E(z'-l'd) = \xi_0^E(z-(l+\frac{1}{2})d)\xi_0^E(z-(l+\frac{1}{2})d)\xi_0^E(z'-(l'+\frac{1}{2})d)\xi_0^E(z'-(l'+\frac{1}{2})d) = EEEE$, $\xi_0^E(z-ld)\xi_0^E(z-ld)\xi_0^E(z'-l'd)\xi_c^I(z'-(l'+\frac{1}{2})d) = EEEI$ and $\xi_0^E(z-ld)\xi_0^E(z-ld)\xi_c^I(z'-(l'+\frac{1}{2})d)\xi_c^I(z'-(l'+\frac{1}{2})a) = EEII$, and so on. The relation

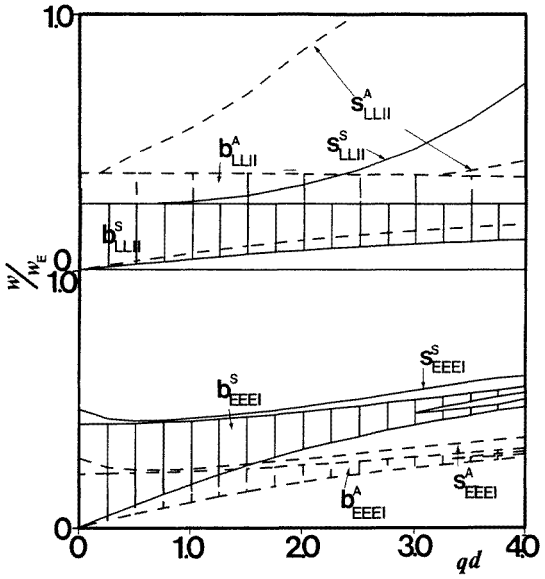

Figure 3. Dispersion relation $\omega/\omega_E = \omega/5\omega_L = \omega/\sqrt{3}\omega_H = \omega/\sqrt{2}\omega_I$ versus qd for intrasubband bulk and surface plasmons modes contributed by $LLII$ (upper section) and $EEEI$ (lower section) states using the symmetric and antisymmetric wavefunctions at the interface states. The parameters used are the same as in figure 1.

$b^{mn}_{EEEE} = \cos(k_z a)$ due to $EEEE$ can be calculated from $\varepsilon(k_z) = \mathbf{\Pi}^0(k_z)/\mathbf{\Pi}^B(k_z)$. The range $-1 < b^{mn}_{EEEE} < 1$ defines the bulk plasmons band which occurs with a fixed q parallel to the layers taking into account k_z. The dispersion of the surface plasmon is obtained from the relation $M(q,\omega) = 0$ which describes the pole of the surface part. The matrix $M(q,\omega)$ is made up of the coefficients A_{11}, A_{12}, A_{21} and A_{22}. For the cases $EEEE$, $LLLL$ and $HHHH$ and $IIII$ using symmetric and antisymmetric interface wavefunctions, the dispersion relations of the intrasubband surface and bulk plasmons are plotted in figure 1. In calculations of the dispersion relations for the various plasmons, conditions such as $\gamma_0/\omega_E = \gamma_E/\omega_E = \gamma_L/\omega_L = \gamma_H/\omega_H = \gamma_I/\omega_I = 0$ are used. Figure 1 which shows $\omega/\omega_E = \omega/5\omega_L = \omega/\sqrt{3}\omega_H = \omega/\sqrt{2}\omega_I$ versus qd for a semi-infinite system illustrates the regions for each mode such as one bulk mode and two surface intrasubband and intersubband modes for the case of $EEEE$ states, one bulk mode and one surface mode for the case of the $HHHH$ state, one bulk mode and two surface modes for the case of $LLLL$ states, and one bulk mode and one surface mode for the case of $IIII$ states calculated using the symmetric and antisymmetric wavefunctions. The conditions $\varepsilon(k_z) = 0$ and $M(q,\omega) = 0$ for the bulk and surface modes are the same as found by others (Jain and Allen 1985a, b, Tzoar and Zhong 1986). S^n_{ijtw} and b^n_{ijtw} stand for the intrasubband and the intersubband of surface modes and the intrasubband and the intersubband of bulk modes, respectively, with the exceptions of S^A_{IIII}, b^A_{IIII}, S^S_{IIII} and b^S_{IIII}, where the superscripts A and S stand for the symmetric and antisymmetric wavefunctions, respectively, of the interface states. S^A_{IIII} modes appear at a larger relative energy value than S^S_{IIII} does. b^A_{IIII} modes appear at larger relative energy than b^S_{IIII} modes do. S^A_{IIII} modes begin to appear from $qd = 0.4$ and have a larger relative energy value than b^A_{IIII} modes do. S^S_{IIII} modes begin to appear from $qd = 2.0$ and have a larger relative energy value than b^S_{IIII} modes do. The two

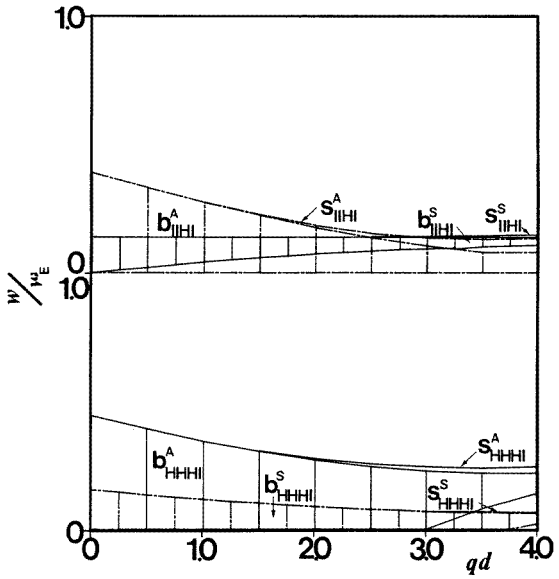

Figure 4. Dispersion relation $\omega/\omega_E = \omega/5\omega_L = \omega/\sqrt{3}\omega_H = \omega/\sqrt{2}\omega_I$ versus qd for intrasubband bulk and surface plasmons modes contributed by $IIHI$ (upper section) and $HHHI$ (lower section) states using the symmetric and antisymmetric wavefunctions at the interface states. The parameters used are the same as in figure 1.

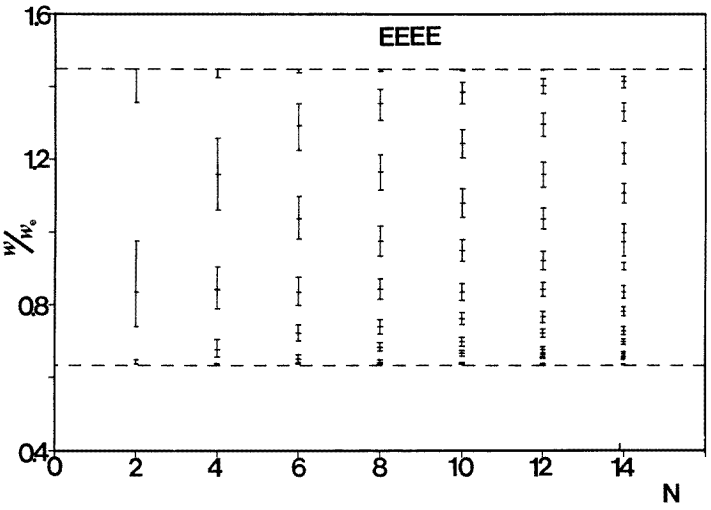

Figure 5. The ratio of energies of modes as a function of the number of unit cells for intrasubband bulk plasmon modes contributed by $EEEE$ states. The broken lines are the band edges of the bulk modes. The parameters used are the same as in figure 1.

intrasubband surface modes S^0_{EEEE} and S^0_{LLLL} are for the electron-like states at $z = ld$ or $z = l(d+\frac{1}{2})$ in HgTe layers and for the light-hole-like states at $z = l(d+\frac{1}{2})$ or $z = l(d+1)$ in CdTe layers. These surface modes begin to appear from $qd = 0.23$. Figure 1 also shows that two intersubband surface modes S^1_{EEEE} begin to appear from $qd = 0.25$. The gap

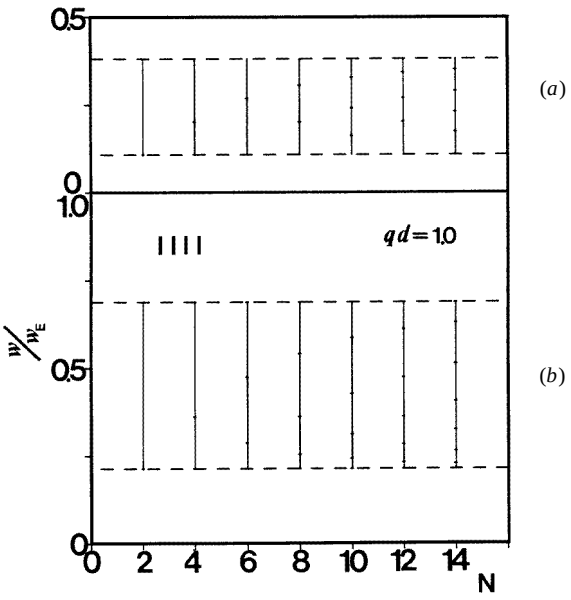

Figure 6. The ratio of energies of modes as a function of the number of unit cells for intrasubband bulk plasmon modes by $IIII$ states using the symmetric (upper section (a)) and the antisymmetric (lower section (b)) wavefunctions of the interface states in the upper and lower boxes. The broken lines are the band edges of the bulk modes. The parameters used are the same as in figure 1.

between S^1_{EEEE} and b^1_{EEEE} modes increases as the value of qd increases. The b^0_{ijtw} modes except for b^0_{HHHH} begin to appear from $qd = 0$. The b^0_{HHHH} modes begin to appear from $qd = 0.7$ and S^0_{HHHH} modes from 0.5.

Figure 2 shows $\omega/\omega_E = \omega/5\omega_L = \omega/\sqrt{3}\omega_H = \omega/\sqrt{2}\omega_I$ versus qd for the cases of $EEII$ and $HHII$ states for a semi-infinite system (Tzoar and Zhang 1986). The shaded regions surrounded by the broken lines are intrasubband modes obtained by the symmetric interface wavefunction. The other regions of the solid lines are intrasubband modes obtained by antisymmetric wavefunctions. b^S_{EEII} modes are the overlapping modes between the electron-like wavefunction and the symmetric interface wavefunction. The b^S_{EEII} modes exist over an energy region larger than that of b^A_{EEII} modes which are the overlapping modes between the electron-like wavefunction and the antisymmetric interface wavefunction. The intrasubband surface modes S^S_{EEII} result from overlap between the electron-like wavefunction and the symmetric interface wavefunction. The S^S_{EEII} modes exist over wavevectors larger than the wavevector $q = 0.95/d$ and over an energy region larger than that of b^S_{EEII} modes. The two intrasubband surface modes S^A_{EEII} result from overlap between the electron-like wavefunction and the antisymmetric interface wavefunction. The S^A_{EEII} modes exist over wavevectors larger than $q = 0.75/d$ and over an energy region larger than that of b^A_{EEII} modes. The b^A_{HHII} modes which are the overlapping modes between the heavy-hole-like states in the HgTe layer and the antisymmetric interface wavefunction exist over energy regions larger than those of b^S_{HHII} modes which result from overlap between the heavy-hole-like state and the symmetric interface wavefunction. The intrasubband surface modes S^S_{HHII} exist over wavevectors larger than $q = 1.46/d$, and an energy region larger than that of b^S_{HHII} modes. The intrasubband surface mode S^A_{HHII}

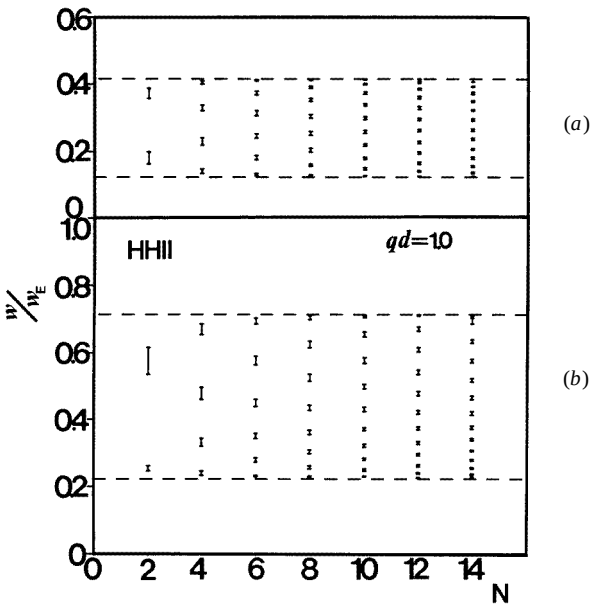

Figure 7. The ratio of energies of modes as a function of the number of unit cells for intrasubband bulk plasmon modes contributed by $HHII$ states using the symmetric (upper section (a)) and the antisymmetric (lower section (b)) wavefunctions of the interface states in the upper and lower boxes. The broken lines are the band edges of the bulk modes. The parameters used are the same as in figure 1.

exists over a wavevector larger than $0.5/d$, and an energy region larger than that of b^A_{HHII} modes. These bulk modes begin to appear from $qd = 0$.

Figure 3 shows $\omega/\omega_E = \omega/5\omega_L = \omega/\sqrt{3}\omega_H = \omega/\sqrt{2}\omega_I$ versus qd for the cases of the $LLII$ and $EEEI$ states (Kim and Sohn 1994). The shaded regions surrounded by the solid lines are the intrasubband modes obtained by the symmetric interface wavefunction. The other regions of the broken lines are the intrasubband modes obtained by the antisymmetric wavefunctions. b^A_{LLII} modes which are the overlap modes between the electron-like state and the antisymmetric interface wavefunction exist over an energy region larger than that of b^S_{LLII} modes, the overlap modes between the electron-like state and the symmetric interface wavefunction. The two intrasubband surface modes S^A_{LLII} exist over wavevectors larger than $q = 0.18/d$ and over an energy region larger than that of b^A_{LLII} modes. The S^S_{LLII} modes begin to appear from $qd = 0.7$. The b^S_{EEEI} modes exist over an energy region larger than that of b^A_{EEEI} modes. The intrasubband surface modes S^S_{EEEI} and S^A_{EEEI} exist over an energy region larger than those of b^S_{EEEI} and b^A_{EEEI}, respectively. These bulk and surface modes begin to appear from $qd = 0$.

Figure 4 shows $\omega/\omega_E = \omega/5\omega_L = \omega/\sqrt{3}\omega_H = \omega/\sqrt{2}\omega_I$ versus qd for the cases of $HHHI$ and $IIHI$ states. S^A_{IIHI} and S^S_{IIHI} modes exist over the wavevectors larger than $q = 1.4/d$ and $2.5/d$, respectively, and S^A_{IIHI} and S^S_{IIHI} over energy regions larger than those of b^A_{IIHI} and b^A_{IIHI} modes, respectively. The S^A_{HHHI} and S^S_{HHHI} modes exist over the wavevectors larger than $q = 1.5/d$ and $q = 2.9/d$, respectively. As the value of qd increases, the value of ω/ω_E decreases for b^A_{HHHI} and b^A_{IIHI} modes.

Figures 5–7 show how the distribution of $\omega/\omega_E = \omega/5\omega_L = \omega/\sqrt{3}\omega_H = \omega/\sqrt{2\omega_I}$ changes with the number N of unit cells. Figure 5 shows ω/ω_E versus N in the case of

the $EEEE$ state. The broken lines in figures 5–7 represent $b^0_{ijtw} = \pm 1.0$ at $qd = 1.0$ for a semi-infinite system. As the number N of the unit cells increases, the number of the bulk plasmon bands increase and the discrete bulk plasmon band is replaced by the continuous bulk plasmon band gradually.

Figures 6(a) and 6(b) show ω/ω_E versus N in the case of $IIII$ states calculated using the symmetric and antisymmetric wavefunctions, respectively, at interface states. The number of doubly degenerate bulk plasmon bands is Int$[(N+2)/6]$ + Int$[(N-2)/6] + 1 (N = 2, 4, 6, \ldots, 14)$ in using the symmetric wavefunction. Here Int$[\cdots]$ means the integer part of real number. The number of doubly degenerate bulk plasmon band is $N/2$ using the antisymmetric wavefunction.

Figures 7(a) and 7(b) show ω/ω_E versus N for $HHII$ states calculated using the symmetric and antisymmetric wavefunctions, respectively, of interface states at $qd = 1.0$. There are two groups of N bulk plasmon bands calculated using the symmetric and antisymmetric wavefunctions at $qd = 1.0$. In figures 6 and 7, the values of the energy modes using the antisymmetric wavefunction are larger than those of modes using the symmetric wavefunction. As the number of unit cells increases, the number of bulk plasmon bands increases and the discrete bulk plasmon band is gradually replaced by the continuous bulk plasmon band as in figure 5. In light scattering, since only a very small exchange of momentum q is accessible, it is desirable to have a large α_0 in order to see the intrasubband surface plasmon.

4. Raman intensities

The Raman intensity is proportional to the function $F(\omega, Q)$ in equation (20). This function contains the imaginary part of the density–density correlation function (Grecu 1973, Fetter 1974). We assume that the incoming light will interact with the carriers of one layer in unit cell. Let the incoming light and the scattered light have frequencies and wavectors (ω_i, q_i, k_z^i) and $(\omega_S, q_S, -k_z^S)$, respectively, at $T = 0$ and let $\omega = \omega_i - \omega_S$ and $Q = (q, k_z) = (q_i - q_S, k_z^i - k_z^S)$. Using the approximation (Kim and Sohn 1994) $k_z^i = k_z^S = k_z + \mathrm{i}/2\lambda$, where $k_z = (\omega_i/c)\,\mathrm{Re}\,\sqrt{\varepsilon}$, and $1/\lambda = (2\omega_i/c)\,\mathrm{Im}\,\sqrt{\varepsilon}$,

$$
\begin{aligned}
F(\omega, Q) = \sum_{n,m}\sum_{l,l'}\sum_{n',m'}\sum_{ijpt} \exp\left(-\frac{2\delta}{\lambda}\right)\int_{-\delta}^{\infty}\int_{-\delta}^{\infty} \mathrm{d}z\,\mathrm{d}z'\,\mathrm{Im}\Big\{ & -\Pi^{0ijpt}_{nm}\varepsilon^{ijpt}_{nm}(l,l';nm)^{-1} \\
& \times \exp[-2\mathrm{i}k_z(z-z')]\exp\left(-\frac{(z+z')}{\lambda}\right) \\
& \times [R^*_{k_z,n}R_{k_z,m} - (\delta_{i,E}\delta_{j,E} + \delta_{i,L}\delta_{j,L} + \delta_{i,H}\delta_{j,H})(R_{k_z,n}R^*_{k_z,m} - 1)] \\
& \times [R^*_{k'_z,n'}R_{k'_z,m'} - (\delta_{t,E}\delta_{w,E} + \delta_{t,L}\delta_{w,L} + \delta_{t,H}\delta_{w,H})(R_{k'_z,n'}R^*_{k'_z,m'} - 1)]V_q \\
& \times \Bigg[\xi^i_n\left(z - ld - \frac{\delta_{i,H}d}{4} - (\delta_{i,L}+\delta_{i,I})\frac{d}{2}\right) \\
& \times \xi^j_m\left(z - l_1 d - \frac{\delta_{j,H}d}{4} - (\delta_{j,L}+\delta_{j,I})\frac{d}{2}\right) + \xi^i_n\left(z - ld - \frac{\delta_{i,E}d}{2} - \delta_{i,L}d\right) \\
& \times \xi^j_m\left(z - l_1 d - \frac{\delta_{j,E}d}{2} - \delta_{j,L}d\right)\Bigg]\Bigg[\xi^t_n\left(z - ld - \frac{\delta_{t,H}d}{4} - (\delta_{t,L}+\delta_{t,I})\frac{d}{2}\right) \\
& \times \xi^w_m\left(z - l_1 d - \frac{\delta_{w,H}d}{4} - (\delta_{w,L}+\delta_{w,I})\frac{d}{2}\right) + \xi^t_n\left(z - ld - \frac{\delta_{t,E}d}{2} - \delta_{t,L}d\right)
\end{aligned}
$$

$$\times\xi_m^w\left(z - l_1 d - \frac{\delta_{w,E} d}{2} - \delta_{w,L} d\right)\Bigg]\Bigg\}$$

$$= \sum_{ijpt}\sum_{nm} \mathrm{Im}\Bigg[- \sum_{l,l'} A_{nm}^{ijpt}\Pi_{nm}^{0ijpt}\varepsilon_{nm}^{ijpt}(l,l';nm)^{-1}\exp(-\mathrm{i}k_z(l-l')a]$$

$$\times \exp\left(\frac{-\mathrm{i}k_z(l+l')a}{\lambda}\right)\Bigg] \tag{20}$$

with an amplitude A_{nm}^{ijpt}. After some rearrangement, equation (20) is expressed by

$$F(\omega, q, k_z) = \sum_{ijpt}\sum_{nm} A_{nm}^{ijpt}\ \mathrm{Im}[-\Pi_{nm}^{0ijpt}\varepsilon_{nm}^{ijpt}(\omega, q, 2k_z)^{-1}] \tag{21}$$

where the effective inverse dielectric function $\varepsilon_{nm}^{ijpt}(\omega, q, 2k_z)^{-1}$ has 121 terms (Kim and Sohn 1994) expressed by i, j, p and t with each designating one state of the electron-like states, the light-hole-like states, the heavy-hole-like state and interface states in the HgTe/CdTe superlattice. $nm = 0$ when $n = m = 0$ or $nm = 1$ when $n = 0$ and $m = 1$ or $n = 1$ and $m = 0$. (Details are given in appendix.) Here, $2k_z$ is the momentum transfer to the plasmon from a photon along the superlattice axis and λ is the photon decay length in superlattice. In calculations for $EEEE$, $LLLL$, $HHHH$ and $IIII$, the imaginary parts of equation (21) become

$$\Pi_{nn}^{0iiii}\varepsilon_{nn}^{iiii}(\omega, q, k_z)^{-1} = \Pi_{nn}^{0iiii}\Bigg(\frac{1}{\gamma_{nn}^{iiii}(1-\exp(-2\delta/\lambda))}$$

$$+\frac{\Pi_{nn}^{0iiii}V_q g_{iiiiM}^{nn}\sinh(qd)\,[U_{nn}^{iiii2}\exp(2d/\lambda)-1]}{\gamma_{nn}^{iiii2}\sqrt{b_{iiii}^{nn2}-1}(1-\exp(-2d/\lambda))E_{nn}^{iiii}}$$

$$+\frac{[1-\exp(-qdN)]\Pi_{nn}^{0iiii}V_q\exp(2d/\lambda)[U_{nn}^{iiii2}A_{11}+(A_{12}+A_{21})U_{nn}^{iiii}+A_{22}]}{4\gamma_{nn}^{iiii2}(b_{iiii}^{nn2}-1)E_{nn}^{iiii}}\Bigg) \tag{22}$$

where

$$E_{nm}^{iiii} = 1 + U_{nm}^{iiii2}\exp(2a/\lambda) - 2U_{nm}^{iiii}\exp(a/\lambda)\cos(2k_z a) \tag{23}$$

$$U_{nm}^{iiii} = b_{iiii}^{nm} - \sqrt{b_{iiii}^{nm2}-1} \qquad (i = E, H, L \text{ and } I) \tag{24}$$

$$b_{ijtw}^{mn} = \cosh(qd) - [g_{ijtwM}^{mn}V_q\sinh(qd)]/\gamma_{mn}^{ijtw} \tag{25}$$

and

$$\gamma_{mn}^{ijtw} = 1 - [g_{ijtw0}^{mn} - g_{ijtwM}^{mn}]V_q\Pi_{mn}^{0ijtw}. \tag{26}$$

When each of i, j, t and w is E, L or H, mn of b_{ijtw}^{mn} and γ_{mn}^{ijtw} is 1 or 0. When each of i, j, t and w stands for I, mn of b_{ujtw}^{mn} is A or S. The other terms can be expressed in a similar manner.

The Raman intensity $F(\omega, q, 2k_z)$ is calculated for $N = 40$ by equation (21) using the following parameters: $k_z = 0.39\times10^8\ \mathrm{m}^{-1}$, $qd = 1.0$, $n = 1.28\times10^{12}\ \mathrm{cm}^{-2}$ and $\gamma_i/\omega_i = 0.2$ with $i = E, L, H$ and I. The calculated spectra are shown in figures 8, 9 and 10. The Raman intensities of bulk and surface states are drawn on two different scales as shown in figures 8, 9 and 10.

Figure 8 shows the Raman intensities of intrasubband bulk and surface for plasmons with the symmetric wavefunction at the interface states. In this figure, the various peaks of

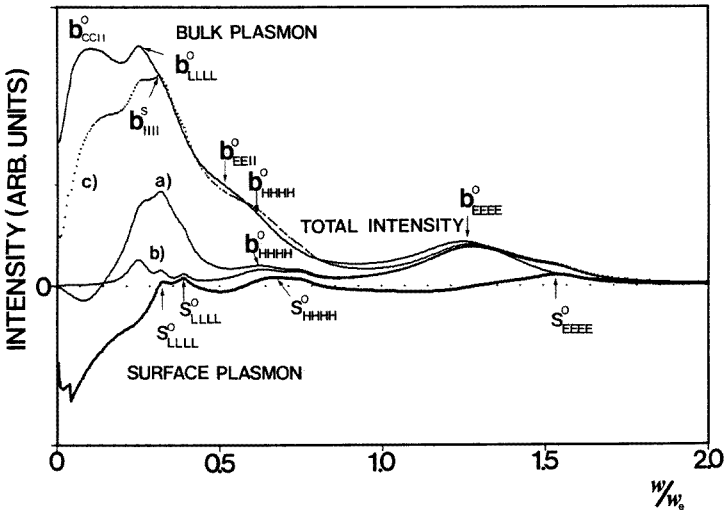

Figure 8. Raman intensities versus $\omega/\omega_e = \omega/5\omega_L = \omega/\sqrt{3}\omega_H = \omega/\sqrt{2}\omega_I$ for the intrasubband bulk and surface plasmons using the symmetric wavefunction at interface states at $qa = 1.0$ and $k_z = 0.39 \times 10^6$ cm^{-1}: (a) the Raman intensities due to $EEEE$, $LLLL$, $HHHH$ and $IIII$ states; (b) the Raman intensities due to $EEEE$, $LLLL$ and $HHHH$ states; (c) the total intensity. The parameters are the same as in figure 1. Additional parameters are $\lambda = 6.0d$ and $\gamma_i/\omega_i = 0.2$ with $i = E, L, H$ and I.

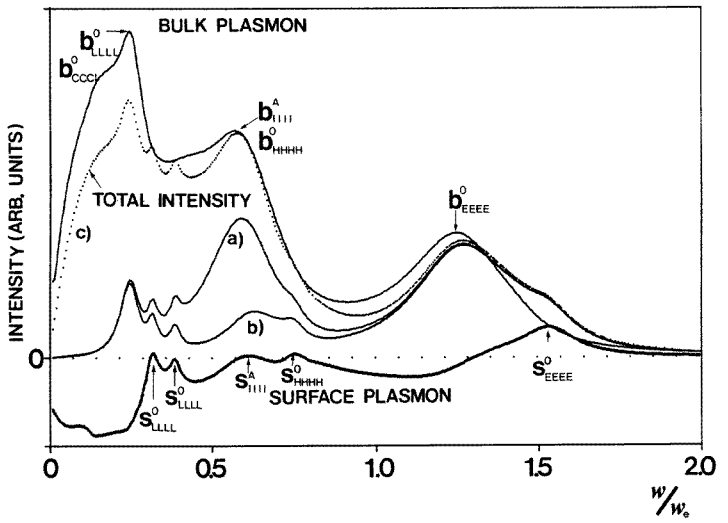

Figure 9. Raman intensities versus $\omega/\omega_E = \omega/5\omega_L = \omega/\sqrt{3}\omega_H = \omega/\sqrt{2}\omega_I$ for the intrasubband bulk and surface plasmons using the antisymmetric wavefunction at the interface states: (a), (b) and (c) have the same meaning as in figure 8. The parameters are the same as in figure 8.

the $EEEE$, $LLLL$, $HHHH$, $IIII$, $EEII$ and $CCII$ states for $N = 40$ are illustrated. Here, $CCII$ states mean the sum of Raman intensities due to $LLII$ and $HHII$ states. The peak at $\omega/\omega_E = 0.105$ is due to the bulk plasmons by $CCII$ states. The peaks

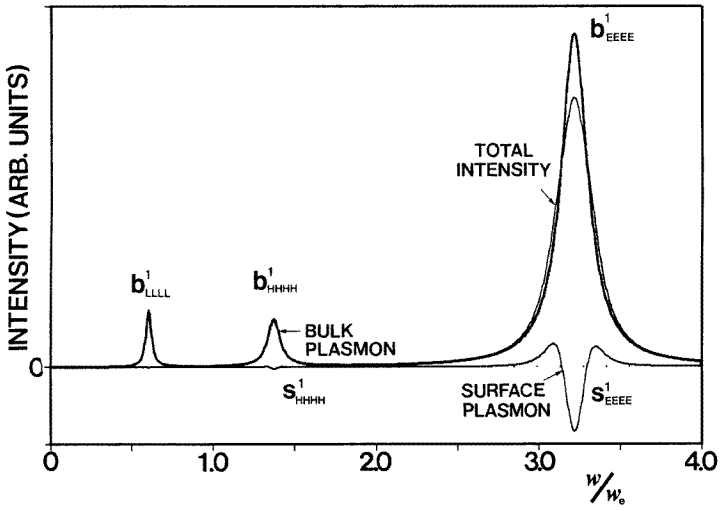

Figure 10. Raman intensities versus $\omega/\omega_E = \omega/5\omega_L = \omega/\sqrt{3}\omega_H = \omega/\sqrt{2}\omega_I$ for the intersubband bulk and surface plasmons. The parameters are the same as in figures 8 and 9 except for $E_{i10} = 2.5\omega_i$ ($i = E, L,$ or H), $\omega_l = 1.8E_{E10}$ and $\omega_T = 1.7E_{E10}$.

at $\omega/\omega_E = 0.25$ and 0.65 are due to the bulk plasmons contributed by $LLLL$ states at $\mathrm{Re}(b^0_{LLLL}) = 1.0$ and by $HHHH$ states at $\mathrm{Re}(b^0_{HHHH}) = 1.0$. The peaks due to the $EEII$ and $IIII$ states appear at $\omega/\omega_E = 0.51$ and 0.315, respectively. The peaks at $\omega/\omega_E = 0.325$ and 0.39 are due to the surface plasmon for two different light hole-like states in the CdTe layers. The surface plasmon contributed by $HHHH$ states occurs at $\omega/\omega_E = 0.67$. The peak at $\omega/\omega_E = 1.245$ is due to the bulk plasmons contributed by $EEEE$ states at $\mathrm{Re}(b^0_{EEEE}) = 1.0$. The surface plasmon contributed by $EEEE$ states occurs at $\omega/\omega_E = 1.535$. The Raman intensities due to $iiiI$ and $iIiI$ ($i = E, L$ and H) states are so small because of weak overlap that the additions of its intensities cause little change to the contributions of $EEEE$, $LLLL$, $HHHH$, $IIII$, $EEII$ and $CCII$ states. Figure 8(a) represents the Raman intensities due to the $EEEE$, $LLLL$, $HHHH$ and $IIII$ states and figure 8(b) represents the Raman intensities due to the $EEEE$, $LLLL$ and $HHHH$ states; figure 8(c) shows the total intensity.

Figure 9 shows the Raman intensities of intrasubband bulk and surface for plasmons with the antisymmetric wavefunction at the interface states. The various peaks due to the $EEEE$, $LLLL$, $HHHH$, $IIII$ and $CCCI$ states using the same parameters as in figure 8 are shown. Here, $CCCI$ states mean the sum of Raman intensities due to the $LLII$, $EEEI$, $HHHI$, and $IIHI$ states. In figure 9, the peak at $\omega/\omega_E = 0.105$ is due to the bulk plasmons contributed by $CCCI$ states. The peak at $\omega/\omega_E = 0.595$ is due to the bulk plasmon contributed by $IIII$ states at $\mathrm{Re}(b^C_{IIII}) = 1.0$. The peak at $\omega/\omega_E = 0.615$ is due to the surface plasmon contributed by $IIII$ states. The locations of the other peaks using the antisymmetric wavefunction of the interface states are the same as those in figure 8 and the magnitude of the b^0_{CCCI} peak is smaller than the b^0_{CCII} peak in figure 8. The peak due to the $IIII$ state in figure 9 appears at a larger value of ω/ω_E than in figure 8. The Raman intensities due to the $HHII$, $EEII$, $LLLI$ and $iIiI$ ($i = E, L$ and H) states are also very small because of weak overlap. As a result, the addition of its intensities change little from the contributions of the $EEEE$, $LLLL$, $HHHH$, $IIII$, $LLII$, $EEEI$, $HHHI$ and $IIHI$ states.

Figure 10 shows the Raman intensities of the intersubband bulk and surface for the electron-like states, light-hole-like states and heavy-hole-like states as functions of ω/ω_E. In figure 10, the various peaks for the intersubband bulk and surface plasmons due to $EEEE$, $LLLL$ and $HHHH$ are illustrated. The two surface and one bulk intersubband states due to $EEEE$, $LLLL$ and $HHHH$, respectively, appear in figure 10. The peak at $\omega/\omega_E = 0.61$ is due to the intersubband bulk plasmon and those at 0.59 and 0.63 are due to the intersubband surface plasmons contributed by $LLLL$ states. The peak at $\omega/\omega_E = 1.38$ is due to the intersubband bulk plasmon and those at 1.335 and 1.425 are due to the intersubband surface plasmons contributed by $HHHH$ states. The peak at $\omega/\omega_E = 3.225$ is due to the intersubband bulk plasmon and those at 3.095 and 3.355 are due to the intersubband surface plasmons contributed by $EEEE$ states.

The magnitude of the peak due to the $EEEE$ states is much larger than those due to the $LLLL$ and $HHHH$ states. In figures 8–10, the important feature is the peaks due to the intrasubband bulk plasmon and intersubband plasmon. The values of ω/ω_E at peaks for the various bulk and surface plasmons in figures 8–10 correspond to those of modes for the various bulk and surface plasmons shown at $qd = 1.0$ in figure 1. These locations of the peaks can be made to shift a little by adjusting the value of k_z. The broadening of the Raman intensity for bulk plasmons is due to photon decay while that for surface plasmons is controlled by α_0.

5. Conclusion

The dispersion relations of collective modes for the electron-like-states, the light-hole-like-states and the heavy-hole-like states in the HgTe/CdTe superlattice have been calculated using the symmetric and antisymmetric wavefunctions at interface states. The calculations have been made under the assumption that only the lowest subband and first excited state are occupied and that interface states between the HgTe and CdTe layers have a symmetric or antisymmetric wavefunction in unit cells. The interface states are located between the HgTe and CdTe layers. The main concern was the overlap between wavefunctions of plasmons and the interface state. Expressions for the interaction potentials and the polarizability matrix of 121 carrier types in unit cells were obtained. The expressions are divided into the bulk and surface parts depending on k_z. After calculation of the dispersion overlap between the interface state and the other plasmon states, intrasubband surface plasmon states show up at larger values of ω/ω_e compared with the bulk plasmon states in the case of the symmetric and antisymmetric wavefunctions of the interface states. The intrasubband surface plasmons S^A_{ijtw} which result from overlap between the antisymmetric interface wavefunction and the other plasmon states begin to appear at a smaller value of qd compared with S^S_{ijtw} which results from overlap between the symmetric interface wavefunction and the other plasmons. The $EEEI$ state, however, is exceptional. In the dispersion spectra of the intersubband bulk and surface plasmon modes for $EEEE$ states, the gap between the two intersubband surface modes S^1_{EEEE} and the intersubband bulk modes b^1_{EEEE} increases as the value of qd increases. Here a large α_0 is needed in order to see the refined intrasubband surface plasmon. The dispersion relations of collective modes contributed by $EEEE$, $IIII$, and $HHII$ states for the symmetric and the antisymmetric wavefunctions at interface states were obtained for intrasubband bulk plasmons as a function of the number of unit cells. For a system of N unit cells, there are N intrasubband bulk mode bands which satisfy the condition $b^{mn}_{ijtw} = \cos(k_z d)$. For the two cases of $EEEE$ and $HHII$ states, the number of the bulk plasmon bands increases as the number of unit cell increases. As the number of unit cells increases, the discrete

bulk plasmon bands become a continuous bulk plasmon band. For the two cases of $IIII$ states for the symmetric and antisymmetric wavefunctions at interface states, the number of doubly degenerate bulk plasmon bands, Int$[(N+2)/6]$ + Int$[(N-2)/6]+1$ and $N/2$, bands were calculated for each wavefunction. In the calculation of Raman intensities as a function of $\omega/\omega_E = \omega/5\omega_L = \omega/\sqrt{3}\omega_H = \omega/\sqrt{2}\omega_I$ for the symmetric and antisymmetric wavefunctions at the interface states, the values of ω/ω_E at peaks for the various bulk and surface plasmons in figures 8–10 correspond to those of modes for the various bulk and surface plasmons shown at $qd = 1.0$ in figure 1. These locations of the peaks can be made to shift a little by adjusting the value of k_z. For the case of the symmetric wavefunction at interface states, the Raman intensities due to $iiiI$ and $iIiI$ states are so small because of weak overlap that the addition of its intensities can make little difference to the sum of intensities due to the $EEEE$, $LLLL$, $HHHH$, $IIII$, $EEII$ and $CCII$ states. For the case of the antisymmetric wavefunction at interface states, the Raman intensities due to $HHII$, $EEII$, $LLLI$ and $iIiI$ states are so small because of weak overlap that the addition of its intensities make little different to the sum of intensities due to the $EEEE$, $LLLL$, $HHHH$, $IIII$, $LLII$, $EEEI$, $HHHI$ and $IIHI$ states. As a result, the contribution to the Raman intensity by the symmetric wavefunction of the interface states is much stronger than the contribution of the antisymmetric wavefunction. In the calculation of Raman intensities of the intersubband bulk and surface for the electron-like states, light-hole-like states and heavy-hole-like states as a function of ω/ω_E, the magnitude of the Raman intensities due to the $EEEE$ states is the largest of all. The broadening of the Raman intensity for bulk plasmons is due to photon decay while that for surface plasmons is controlled by α_0.

Acknowledgments

This work was supported in part by the Non Directed Research Fund, Korea Research Foundation (1995) and by the Korea Science and Engineering Foundation through the Atomic-scale Surface Science Research Center at Yonsei University (1995).

Appendix 1

The bulk parts of $V^{ijtw}_{nm,nm}(k_z, k'_z)$ are (Kim and Sohn 1994, Eliasson *et al* 1987)

$$V^{Bijtw}_{nm,nm}(k_z) = \left(\frac{\sinh(qd)}{P(k_z)} - 1\right) g^{nm}_{ijtwM}(q) + g^{nm}_{0ijtw}(q) \tag{A1.1}$$

where

$$\begin{aligned} g^{nm}_{ijtwM}(q) = \int \Bigg[& \xi^i_n\left(z - ld - \frac{\delta_{i,H}d}{4} - (\delta_{i,L}+\delta_{i,I})\frac{d}{2}\right)\xi^j_m\left(z - l_1 d - \frac{\delta_{j,H}d}{4} - (\delta_{j,L}+\delta_{j,I})\frac{d}{2}\right) \\ & + \xi^i_n\left(z - ld - \frac{\delta_{i,E}d}{2} - \delta_{i,L}d\right)\xi^j_m\left(z - l_1 d - \frac{\delta_{j,E}d}{2} - \delta_{j,L}d\right)\Bigg] \\ & \times \exp[-q(z-z')]\Bigg[\xi^t_n\left(z - ld - \frac{\delta_{t,H}d}{4} - (\delta_{t,L}+\delta_{t,I})\frac{d}{2}\right) \\ & \times \xi^w_m\left(z - l_1 d - \frac{\delta_{w,H}d}{4} - (\delta_{w,L}+\delta_{w,I})\frac{d}{2}\right) + \xi^t_n\left(z - ld - \frac{\delta_{t,E}d}{2} - \delta_{t,L}d\right) \\ & \times \xi^2_m\left(z - l_1 d - \frac{\delta_{w,E}d}{2} - \delta_{w,L}d\right)\Bigg] \mathrm{d}z\, \mathrm{d}z' \end{aligned} \tag{A1.2}$$

$$g^{nm}_{0ijtw}(q) = \int \left[\xi^i_n\left(z - ld - \frac{\delta_{i,H}d}{4} - (\delta_{i,L}+\delta_{i,I})\frac{d}{2}\right)\xi^j_m\left(z - l_1 - \frac{\delta_{j,H}d}{4} - (\delta_{j,L}+\delta_{j,I})\frac{d}{2}\right)\right.$$
$$\left.+\xi^i_n\left(z - ld - \frac{\delta_{i,E}d}{2} - \delta_{i,L}d\right)\xi^j_m\left(z - l_1 d - \frac{\delta_{j,E}d}{2} - \delta_{j,L}d\right)\right]$$
$$\times \exp(-q|z-z'|)\left[\xi^t_n\left(z - ld - \frac{\delta_{t,H}d}{4} - (\delta_{t,L}+\delta_{t,I})\frac{d}{2}\right)\right.$$
$$\times\xi^2_m\left(z - l_1 d - \frac{\delta_{w,H}d}{4} - (\delta_{w,L}+\delta_{w,I})\frac{d}{2}\right) + \xi^t_n\left(z - ld - \frac{\delta_{t,E}d}{2} - \delta_{t,L}d\right)$$
$$\left.\times\xi^w_m\left(z - l_1 d - \frac{\delta_{w,E}d}{2} - \delta_{w,L}d\right)\right]\mathrm{d}z\,\mathrm{d}z' \qquad \text{(A1.3)}$$

$$g^{nm}_{ijtwP}(q) = \int \left[\xi^i_n\left(z - ld - \frac{\delta_{i,H}d}{4} - (\delta_{i,L}+\delta_{i,I})\frac{d}{2}\right)\xi^j_m\left(z - l_1 d - \frac{\delta_{j,H}d}{4} - (\delta_{j,L}+\delta_{j,I})\frac{d}{2}\right)\right.$$
$$\left.+\xi^i_n\left(z - ld - \frac{\delta_{i,E}d}{2} - \delta_{i,L}d\right)\xi^j_m\left(z - l_1 d - \frac{\delta_{j,E}d}{2} - \delta_{j,L}d\right)\right]$$
$$\times \exp[-q(z+z')]\left[\xi^t_n\left(z - ld - \frac{\delta_{t,H}d}{4} - (\delta_{t,L}+\delta_{t,I})\frac{d}{2}\right)\right.$$
$$\times\xi^w_m\left(z - l_1 d - \frac{\delta_{w,H}d}{4} - (\delta_{w,L}+\delta_{w,I})\frac{d}{2}\right) + \xi^t_n\left(z - ld - \frac{\delta_{t,E}d}{2} - \delta_{t,L}d\right)$$
$$\left.\times\xi^w_m\left(z - l_1 d - \frac{\delta_{w,E}d}{2} - \delta_{w,L}d\right)\right]\mathrm{d}z\,\mathrm{d}z'. \qquad \text{(A1.4)}$$

The E, L, H and I indicate electron-like state, light-hole-like state and heavy-hole-like state and interface state, respectively. For instance, in the case of I, the subscripts nm of functions ξ^i_n, ξ^j_m, ξ^t_n and ξ^w_m represent C. C is either A or S where A and S correspond to the antisymmetric wavefunction and the symmetric wavefunction, respectively, at interface states.

Appendix 2

$V^{ijtw}_{nm,n'm'}(l,l_1,l',l'_1)$ in equation (6) is as follows:

$$V^{ijtw}_{nm,n'm'}(l,l_1,l',l'_1) = [R^*_{k_z,n}R_{k_z,m} - (\delta_{i,E}\delta_{j,E}+\delta_{i,L}\delta_{j,L}+\delta_{i,H}\delta_{j,H})(R_{k_z,n}R^*_{k_z,m}-1)]$$
$$\times[R^*_{k'_z,n'}R_{k'_z,m'} - (\delta_{t,E}\delta_{w,E}+\delta_{t,L}\delta_{w,L}+\delta_{t,H}\delta_{w,H})(R_{k'_z,n'}R^*_{k'_z,m'}-1)]V_q$$
$$\times\int_{-\delta}^{\infty}\mathrm{d}z\int_{-\delta}^{\infty}\mathrm{d}z\left[\xi^i_n\left(z - ld - \frac{\delta_{i,H}d}{4} - (\delta_{i,L}+\delta_{i,I})\frac{d}{2}\right)\right.$$
$$\times\xi^j_m\left(z - l_1 d - \frac{\delta_{j,H}d}{4} - (\delta_{j,L}+\delta_{j,I})\frac{d}{2}\right) + \xi^i_n\left(z - ld - \frac{\delta_{i,E}d}{2} - \delta_{i,L}d\right)$$
$$\left.\times\xi^j_m\left(z - l_1 d - \frac{\delta_{j,E}d}{2} - \delta_{j,L}d\right)\right]\{\exp(-q|z-z'|) + \alpha_1\exp[-q(z+z)]\}$$
$$\times\left[\xi^t_n\left(z - ld - \frac{\delta_{t,H}d}{4} - (\delta_{t,L}+\delta_{t,I})\frac{d}{2}\right)\xi^w_m\left(z - l_1 d - \frac{\delta_{w,H}d}{4} - (\delta_{w,L}+\delta_{w,I})\frac{d}{2}\right)\right.$$
$$\left.+\xi^t_n\left(z - ld - \frac{\delta_{t,E}d}{2} - \delta_{t,L}d\right)\xi^w_m\left(z - l_1 d - \frac{\delta_{w,E}d}{2} - \delta_{w,L}d\right)\right]. \qquad \text{(A2.1)}$$

Here $R_{k_z,n} = [1 + \alpha_{n1} + \alpha_{n2} + \beta_{n1} + \beta_{n2} + \gamma_{nc}]^{-1/2}$ is a renormalization coefficient (Kim and Sohn 1994), which includes the overlap of wavefunctions of the electron-like states, heavy-hole-like states and light-hole-like states with the interface states:

$$\alpha_{n1} = \int \xi_n^E(z - ld)\xi_c^I(z - (l + \tfrac{1}{2})d)\,\mathrm{d}z \tag{A2.2}$$

$$\alpha_{n2} = \int \xi_n^E(z - (l + \tfrac{1}{2})d)\xi_c^I(z - (l + \tfrac{1}{2})d)\,\mathrm{d}z \tag{A2.3}$$

$$\beta_{n1} = \int \xi_n^L(z - (l + \tfrac{1}{2})d)\xi_c^I(z - (l + \tfrac{1}{2})d)\,\mathrm{d}z \tag{A2.4}$$

$$\beta_{n2} = \int \xi_n^L(z - (l + \tfrac{1}{2})d)\xi_c^I(z - (l + 1)d)\,\mathrm{d}z \tag{A2.5}$$

$$\gamma_{nc} = \int \xi_n^H(z - (l + \tfrac{1}{4})d)\xi_c^I(z - (l + \tfrac{1}{2})d)\,\mathrm{d}z. \tag{A2.6}$$

The surface parts of $V_{nm,nm}^{ijtw}(k_z, k_z')$ are

$$\begin{aligned} V_{nmnm}^{Sijtw}(k_z, k_z') = {} & \frac{1 - \exp(-qdN)}{4NP(k_z)P(k_z')} \\ & \times [R_{k_z,n}^* R_{k_z,m} - (\delta_{i,E}\delta_{j,E} + \delta_{i,L}\delta_{j,L} + \delta_{i,H}\delta_{j,H})(R_{k_z,n}R_{k_z,m}^* - 1)] \\ & \times [R_{k_z',n'}^* R_{k_z',m'} - (\delta_{t,E}\delta_{w,E} + \delta_{t,L}\delta_{w,L} + \delta_{t,H}\delta_{w,H})(R_{k_z',n'}R_{k_z',m'}^* - 1)] \\ & \times \{A_{11} + A_{12}\exp(-\mathrm{i}k_z'd) + A_{21}\exp(\mathrm{i}k_z d) + A_{22}\exp[\mathrm{i}(k_z - k_z')d]\}. \end{aligned} \tag{A2.7}$$

References

Berrior J M, Guldner Y and Voos M 1986 *IEEE J. Quantum Electron.* **QE-22** 1793
Chang L L and Esaki L 1980 *Surf. Sci.* **98** 70
Chang Y C, Schulman J N, Bastard G, Guldner Y and Voos Y 1985 *Phys. Rev.* B **31** 2557
Das Sarma S and Quinn J J 1982 *Phys. Rev.* B **25** 7603
Dingle R, Sturmer H L, Gossard A C and Wiegmann W 1980 *Surf. Sci.* **98** 90
Eliasson G, Hawrylak P and Quinn J J 1987 *Phys. Rev.* B **35** 5569
Esaki L and Tsu R 1970 *IBM J. Res. Dev.* **14** 61
Fauri J P 1986 *IEEE J. Quantum Electron.* **QE-22** 1656
Fetter A L 1974 *Ann. Phys., NY* **88** 1
Giuliani G F and Quinn J J 1983 *Phys. Rev. Lett.* **51** 919
Grecu D 1973 *Phys. Rev.* B **8** 1958
Guldner Y, Bastard G and Voos M 1985 *J. Appl. Phys.* **57** 1403
Hawrylak P, Eliasson G and Quinn J J 1986 *Phys. Rev.* B **34** 5368
Hawrylak P, Wu J W and Quinn J J 1985a *Phys. Rev.* B **31** 7855
——1985b *Phys. Rev.* B **32** 4272, 5162
Huang D H, Ping J P and Zhou S X 1989 *Phys. Rev.* B **40** 7754
Huang D H and Zhou S X 1988 *Phys. Rev.* B **38** 13 061, 13 069
Jain J K and Allen P B 1985a *Phys. Rev. Lett.* **54** 947
——1985b *Phys. Rev.* B **32** 997
Jaros M, Zoryk A and Ninno D 1987 *Phys. Rev.* B **35** 8227, 8277
Kim S W and Sohn K S 1994 *Phys. Rev.* B **50** 17 185
Lin-Lin Y C and Sham L J 1985 *Phys. Rev.* B **32** 5561
Mukherji D and Nag B R 1957 *Phys. Rev.* B **12** 4338
Olego D, Pinczuk A, Gossard A C and Wiegmann W 1982 *Phys. Rev.* B **25** 7867
Pinczuk A, Lamont M G and Gossard A C 1986 *Phys. Rev. Lett.* **56** 2092
Sooryakumar R, Pinczuk A, Gossard A and Wiegmann W 1985 *Phys. Rev.* B **31** 2578
Tselis A C and Quinn J J 1984 *Phys. Rev.* B **29** 3318
Tzoar N and Zhang C 1986 *Phys. Rev.* B **34** 1050